Controlling the Spacing of Streamwise Vortices on Concave Walls

Roy Y. Myose* and Ron F. Blackwelder†
University of Southern California, Los Angeles, California 90089

The wavelength of Görtler streamwise vortices was changed by a factor of three by varying the amount of tunnel side wall boundary-layer removal just upstream of the concave wall test section's leading edge. Nondimensional wavelengths in the range $215 \leq \Lambda \leq 900$ were achieved with the larger wavelengths resulting from increased suction. The minimum wavelength compares well with the maximum amplification curve based on past theoretical studies. Low-speed streaks appeared to merge with other low-speed streaks or were weakened to the point of disappearing as the suction level was increased. The downstream location of secondary instability onset changed with variation in suction level and/or wavelength. The Görtler number and amplification factor for secondary instability onset, however, was approximately independent of suction level and/or wavelength.

Nomenclature

A = nondimensional amplification factor, $\exp[\int(4/3)(\beta\theta/G\ddot{o}_\theta)\, dG\ddot{o}_\theta]$
A^* = dimensional amplification factor, $\exp[\int\beta\, dx]$
$G\ddot{o}_\theta$ = Görtler number, $(U_\infty\theta/\nu)\sqrt{\theta/R}$
k = dimensional wave number
R = concave wall radius of curvature
$\bar{u}$ = average streamwise velocity
U_G = average velocity in boundary-layer suction device (BLSD) gap
U_∞ = freestream velocity
X,Y,Z = streamwise, normal, and spanwise distance
β = dimensional amplification rate
δ = boundary-layer thickness
θ = momentum thickness
λ = dimensional spanwise wavelength
Λ = nondimensional spanwise wavelength, $(U_\infty\lambda/\nu)\sqrt{\lambda/R}$
ν = kinematic viscosity

Introduction

BOUNDARY-LAYER flow over concave walls develop counter-rotating streamwise vortices. Görtler[1] and others[2-4] have successfully explained the causal instability mechanism, and experiments[5-14] have confirmed the existence of these so-called Görtler streamwise vortices. However, theory and experiment have been unable to predict or explain the observed vortex wavelength. The following experiment provides additional information on the wavelength selection mechanism and presents a method to control the wavelength of Görtler vortices.

The stability of concave wall flow is governed by the nondimensional parameter given by

$$G\ddot{o}_\theta \equiv (U_\infty\theta/\nu)\sqrt{\theta/R} \tag{1}$$

A disturbance with wave number k is amplified with amplification rate $\beta > 0$ when the Görtler number $G\ddot{o}_\theta$ exceeds the neutral stability curve. Once beyond the neutral stability curve, counter-rotating streamwise vortices are formed and then develop downstream. The nondimensional wavelength of the Görtler vortices is given by

$$\Lambda \equiv (U_\infty\lambda/\nu)\sqrt{\lambda/R} \tag{2}$$

where λ is the observed dimensional wavelength. According to theory,[1-4] all vortices with wavelength greater than $\Lambda \sim 50$ experience amplification. Floryan and Saric[3,4] found the maximum amplification curve to be approximately near the line $\Lambda = 200$. If the Görtler vortices developed along the maximum amplification curve as one might expect from theory, then the selected wavelength should be $\Lambda \approx 200$. However, this is not the case for most experiments[9-12,14]; the wavelengths are much larger and lie in the range $600 \leq \Lambda \leq 2400$. The few exceptions include Bippes[5] with $\Lambda \approx 200$ for a water-towing facility, Winoto and Crane[6] in another water facility with $\Lambda = 200$ to 500, Ito[7] with $\Lambda = 320$, Aihara and Koyama[8] with $\Lambda = 330$, and the present study. Consequently, theory has not been able to predict the observed wavelength nor to explain the large scatter of wavelengths in experiments. This may be due to the fact that the Görtler instability mechanism is very weak at the upstream location where the vortex wavelength is selected.[4] Thus, some other parameter yet to be examined may be required to explain the selected wavelength.

Tani[9] and Tani and Sakagami[10] found in their experimental studies that the physical wavelength λ was independent of downstream location or freestream velocity, but changed when a different experimental facility was used. Consequently, Tani and Sakagami[10] conjectured that the wavelength depends upon the initial disturbance conditions present within the particular wind tunnel being used. Bippes[5] achieved a wavelength of $\Lambda \approx 200$ irrespective of radius of curvature or freestream velocity by imposing an isotropic disturbance field upstream. Bippes' work suggests that the selected wavelength follows the maximum amplification curve predicted by theory *if* the initial disturbance conditions are isotropic. This is to be expected since an isotropic disturbance field would eliminate any preferential wave number present in the experimental facility, and thereby allow wave numbers along the maximum amplification curve to be preferred over others. However, this does not explain what types of disturbances cause deviations from the maximum amplification curve nor how strongly they deviate.

Swearingen and Blackwelder[11] found the average wavelength λ to be independent of screen geometry, test section spanwise width, effective turbulence damping distance, or the

Received June 1, 1990; revision received Dec. 5, 1990; accepted for publication Dec. 17, 1990.

*Research Assistant, Department of Aerospace Engineering. Member AIAA.

†Professor, Department of Aerospace Engineering. Associate Fellow AIAA.

presence of honeycomb in the settling chamber. However, they found that the particular details of the spanwise pattern depend strongly on the last settling chamber screen used. Swearingen and Blackwelder also introduced small-scale disturbances (either 80-μm-thick cellophane tapes on the concave wall near the leading edge or 100-μm-diam cylinders upstream of the leading edge), periodic in the spanwise direction. They found that the wavelength was affected only if the disturbance spacing was less than the naturally occurring wavelength. Tani and Aihara[12] introduced larger-scale disturbances consisting of a row of wings (0.8 cm chord, 2 cm span at 3-deg angle of attack) located outside the boundary layer. They found the resulting wavelength to be aligned with the wing spacing which was twice the naturally occurring wavelength. Bippes[5] used heated wires in his water-towing facility to produce specific wavelengths of $\Lambda = 46$, 147, and 393. Aihara et al.[13] placed a row of wings (at zero angle of attack) upstream of the concave wall leading edge in a water-towing facility. By varying the spanwise spacing of the wings, they were able to obtain desired wavelengths for their investigation of the Görtler stability diagram. With the exception of such limited artificial means, no one has yet succeeded in explaining the selection of or controlling the Görtler wavelength. Such control is desirable and may be especially useful for experiments that require a specific wavelength.

Experimental Setup and Procedure

The experiment was conducted in a low-turbulence, open return wind tunnel.[14] The test section consists of a concave wall with 320-cm radius of curvature, channel width of 15 cm, and spanwise width of 122 cm. The facility includes a boundary-layer suction device (BLSD) shown schematically in Fig. 1a, which is used to remove the tunnel side wall turbulent boundary layer. The BLSD consists of a slot, concentric with the leading edge of the test section, which leads into a plenum chamber connected to an adjustable speed auxiliary fan. Note that the BLSD removes fluid tangentially, i.e., not normal to the surface.

A "sheet of smoke" was introduced at $X = 21.5$ cm and $Y = 0.14$ cm ($Y/\delta_{Blasius} \approx 0.35$) using the smoke-wire technique.[10,14] Flow visualization of the smoke patterns were recorded with a video system as the BLSD auxiliary fan power level was varied. The power levels were later correlated with the flow rate of the outtake hose on the concave side of the BLSD. The flow rate was calculated from pitot tube velocity measurements in the outtake hose based upon a (measured) fully developed turbulent profile. The average gap velocity U_G (see Fig. 1b) was computed from the flow rate using the dimensions of the outtake hose and the BLSD slot gap width. The freestream velocity U_∞ was measured in the test section (at $X = 10$ cm, $Y = 7.5$ cm, $Z = -45$ cm) and maintained constant at $U_\infty = 500$ cm/s throughout the experiment. Data was taken for suction levels resulting in velocity ratios in the range $0.61 \leq U_G/U_\infty \leq 1.92$. Note that an increase in suction results in a larger velocity ratio.

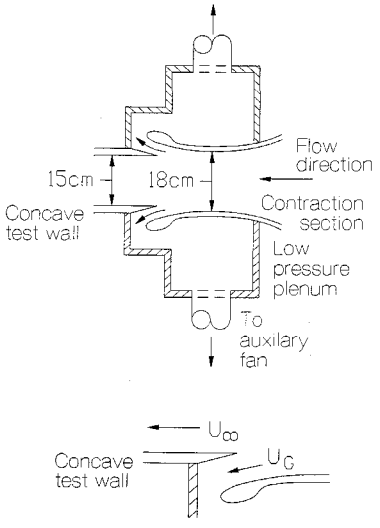

Fig. 1 Schematic of boundary-layer suction device.

Discussion of Results

Figure 2 shows typical flow visualization between $0 \leq Z \leq 20$ cm for two different velocity ratios. The grid lines shown are spaced 10 cm apart in the X and Z directions, and the numbers along the centerline ($Z = 0$ cm) denote downstream distance X in centimeters from the leading edge. The white-smoke filaments coalesce to the low-speed regions known as low-speed streaks that form between pairs of counter-rotating streamwise vortices. Consequently, the average spacing of the low-speed streaks is synonymous with the Görtler wavelength λ. A limited spanwise range of hot-wire velocity data is also shown. The flow visualization and hot-wire velocity data (in Fig. 2) show that the smoke does correlate with the low-speed regions, and the location and average spacing of the low-speed streaks change when the velocity ratio is varied.

The spanwise location of the low-speed streaks were identified from the flow-visualization photographs, and the results are shown in Fig. 3 as a function of velocity ratio. Some low-speed streaks appear faint in the flow-visualization photographs. An example of a faint low-speed streak is indicated by an arrow in Fig. 2b at $Z \approx 9$ cm. These faint low-speed streaks either merge with other low-speed streaks or simply disappear at the next higher velocity ratio.

The Görtler wavelength λ, synonymous with the average spacing of low-speed streaks, was computed from the low-speed streak location information of Fig. 3 and were plotted in Fig. 4. The nondimensional wavelength Λ ($\sim \lambda^{3/2}$) is also shown for reference. Below a velocity ratio of $U_G/U_\infty = 0.76$, the flow was turbulent due to insufficient removal of the tur-

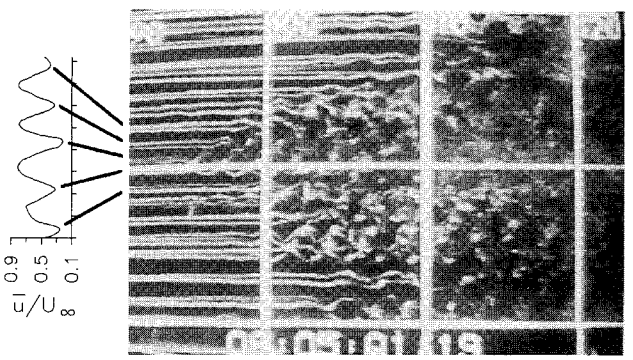

a) Low-speed streaks at $U_G/U_\infty = 0.761$ velocity ratio

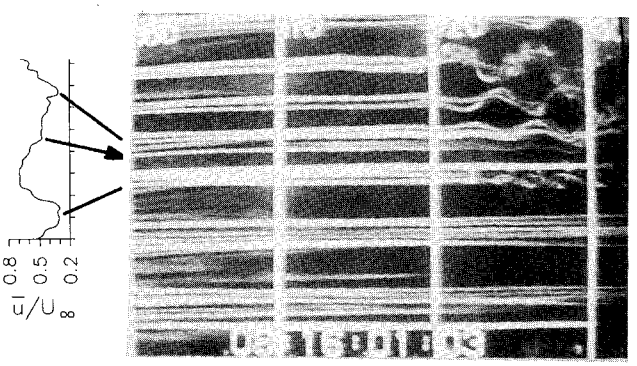

b) Low-speed streaks at $U_G/U_\infty = 0.928$ velocity ratio

Fig. 2 Low-speed streaks for two suction levels. Hot-wire data shown on the left were taken at $X = 83$ cm and $Y = 0.3$ cm.

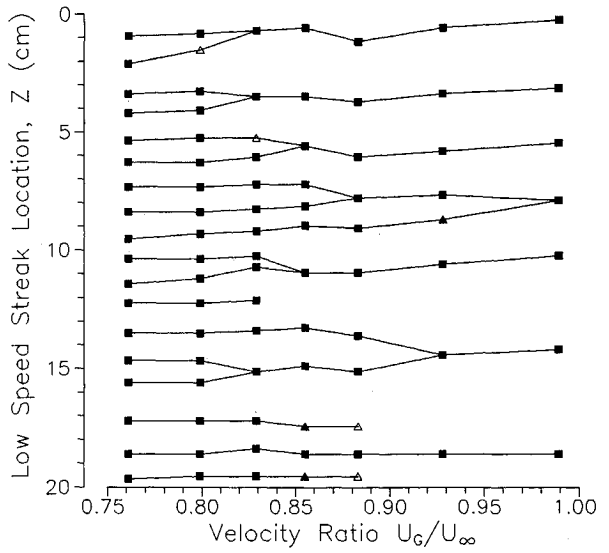

Fig. 3 Low-speed streak location as a function of BLSD gap velocity to freestream velocity ratio. ■: low-speed streak; ▲: faint low-speed streak, included in the average spacing count; △: very faint low-speed streak, excluded from the average spacing count.

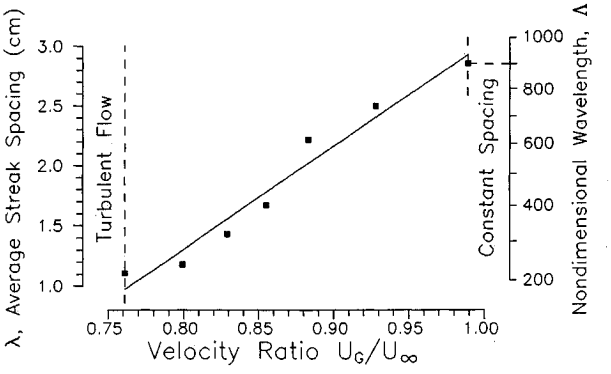

Fig. 4 Average spacing of low-speed streaks (i.e., Görtler wavelength λ) as a function of BLSD gap velocity to freestream velocity ratio.

bulent boundary layer that developed along the wind-tunnel side walls. Above a velocity ratio of $U_G/U_\infty \sim 1$, the average spacing remained relatively constant (at 8 ± 1 low-speed streaks) up through the maximum velocity ratios attempted ($U_G/U_\infty \approx 1.92$). In between, the Görtler vortex wavelength λ increased with the velocity ratios (i.e., suction levels) were increased.

Effect of Wavelength Variation on Secondary Instability

Immediately prior to transition to turbulence, Görtler flow undergoes secondary instability in the form of sinuous motion of the low-speed streaks.[14] The flow-visualization information such as those shown in Fig. 2 revealed that the downstream location of sinuous motion onset was apparently affected. Figure 2a shows an average streamwise location of $X \approx 100$ cm for the onset of sinuous motion of the low-speed streaks. Figure 2b, on the other hand, shows a much further downstream location for the onset of sinuous motion. The location of sinuous motion was generally delayed further downstream as suction level (and resulting wavelength) was increased. Figure 5 shows this trend nondimensionally in the stability diagram. The onset of sinuous motion occurred at a Görtler number (based on Blasius boundary-layer momentum thickness) of $G\ddot{o}_\theta \sim 7.1$ to 8.1 with slight increases for larger wavelengths. These onset locations corresponded to nondimensional amplification rates in the range $5.5 \leq \beta\theta \leq 7.5$. The amplification rates, however, do not indicate the net

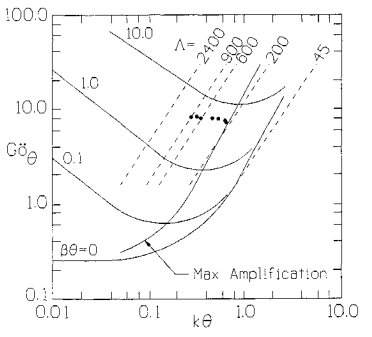

Fig. 5 Stability diagram, curves of constant amplification rate as a function of Görtler number $G\ddot{o}_\theta$, and nondimensional wave number $k\theta = (2\pi/\lambda)\theta$. ——: curves of constant amplification rate from Floryan and Saric[3]; ●: average location of sinuous motion onset for various velocity ratios from present study.

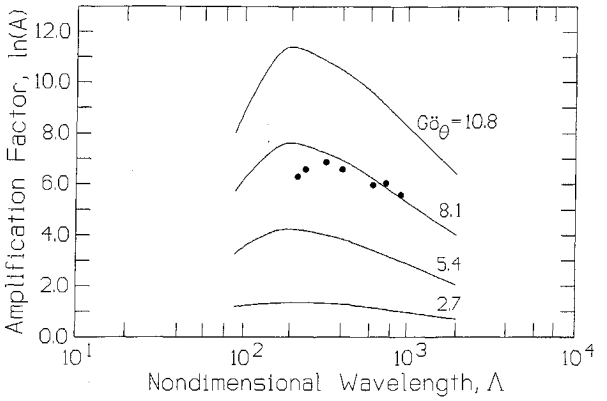

Fig. 6 Curves of total growth of vortices as a function of nondimensional wavelength Λ. ——: curves of total growth from Floryan and Saric[4]; ●: average location of sinuous motion onset for various velocity ratios from present study.

amount of growth undergone by the vortices, but instead indicate the local growth rates. As Fig. 5 shows, Görtler vortices with wavelengths $\Lambda > 200$ undergo slower amplification at the same Görtler numbers. The total amount of growth necessary to trigger sinuous motion is shown in Fig. 6. The curves, showing the net amplification that Görtler vortices with wavelength Λ have undergone by Görtler numbers $G\ddot{o}_\theta$, are due to theoretical calculations by Floryan and Saric.[4] Here, the amplification factor A is given by

$$A = \exp\left(\int_{G\ddot{o}_{\theta,o}}^{G\ddot{o}_\theta} \frac{4}{3}\frac{\beta\theta}{G\ddot{o}_\theta}\, dG\ddot{o}_\theta\right) \tag{3}$$

where $G\ddot{o}_{\theta,o}$ is the Görtler number for neutral stability at the wavelength Λ. Figure 6 shows that an amplification factor in the range $e^{5.5} \leq A \leq e^7$ is necessary for the onset of sinuous motion at the present facility. Thus, sinuous motion appears to occur at a constant Görtler number and/or when the vortices have been amplified by roughly the same net amount. However, the particular value for any given wind tunnel may be facility and/or freestream turbulence-level dependent since low-speed streaks in Ito's facility[7] undergo sinuous motion at $G\ddot{o}_\theta \sim 9.5$ and $A \sim e^9$.

Although data on the onset of secondary instability as a function of wavelength is not available in the literature, there is information on transition locations as a function of nondimensional wavelength. Liepmann[15] found that Görtler flow transitions to turbulence at $G\ddot{o}_\theta = 9$ for low levels of freestream turbulence. Smith,[16] using a concept similar to Floryan and Saric's[4] net amplification factor, found that concave wall boundary layers transition to turbulence when the vortices

were amplified to $A^* = e^9$. Here, Smith's amplification factor A^* is given by

$$A^* = \exp\left(\int_{X_o}^{X_t} \beta \, dx\right) \tag{4}$$

where X_o is the downstream location of Görtler neutral stability and X_t is the downstream location of transition. Note that Liepmann's experiment and Smith's survey of transition experiments on concave airfoil surfaces were made at many different freestream velocities. Tani and Sakagami[10] found that λ is invariant with freestream velocity; this means that a change in U_∞ changes the nondimensional wavelength Λ by a proportionate amount. This implies that Liepmann's and Smith's results were made over many different nondimensional wavelengths. Therefore, the transition Görtler number and amplification factor is apparently independent of the nondimensional wavelength Λ for a given wind-tunnel facility and freestream turbulence level. More direct evidence is provided by Winoto and Low[17] who measured the transition locations at three different freestream velocities (U_∞ = 570, 800, and 1180 cm/s). Since Winoto and Low found the physical wavelength to be relatively constant (at $\lambda = 1.65 \pm 0.15$ cm), the different freestream velocities correspond to a change in nondimensional wavelength (of Λ = 805, 1130, and 1670). They found that the transition Görtler number (based on Blasius boundary-layer momentum thickness) was $G\ddot{o}_\theta = 8$ and that the transition locations based on Smith's $A^* = 9$ prediction were within 2–6.5% of those found in their experiment.

Therefore, the present results along with Winoto and Low's results indicate that nonlinear behavior (i.e., secondary instability and transition) occur independent of Λ at roughly a constant Görtler number and/or when the vortices have been amplified by roughly the same net amount.

Past experimental studies have shown two types of secondary instability modes. In the horseshoe vortex mode, spanwise vortices bridging the pair of Görtler streamwise vortices form as a result of high $\partial u/\partial y$ shear at the inflection point of u velocity vertical profile. Flow visualization of the horseshoe vortex mode has been well documented by Ito[7] as well as many others.[5,8,13,14] Sinuous motion of the low-speed streaks result from high $\partial u/\partial z$ shear at the u velocity spanwise profile inflection point. The sinuous motion mode was investigated in detail by Swearingen and Blackwelder.[14] Bippes,[18] based on his heated-wire experiments,[5] found that the sinuous motion secondary instability mode dominated for the smaller wavelengths. In a numerical modeling study, Park[19] also found the sinuous motion mode to be dominant for smaller wavelengths. In the present experiment, all secondary instability modes were of the pure sinuous motion type until at least Λ = 400. Combination[14] (sinuous and horseshoe) modes began to appear at $\Lambda > 600$ and some pure horseshoe vortex modes at $\Lambda > 700$. Therefore, the present result also supports the view that sinuous motion secondary instability mode dominates for small wavelengths.

Conclusions

The wavelength of Görtler vortices was successfully controlled by varying the suction level of the boundary-layer suction device in this experiment. Nondimensional wavelengths in the range $215 \leq \Lambda \leq 900$ were achieved. The minimum Λ of 215 compares well with $\Lambda \approx 200$ for an isotropic disturbance field of Bippes and the maximum amplification curve of Floryan and Saric. Low-speed streaks appeared to merge with other low-speed streaks or were weakened to the point of disappearing as the suction level was increased. The downstream location of low-speed streak sinuous motion was also affected as a consequence of the variation in wavelength and/or as a result of change in suction level. The sinuous motion began, on average, at a Görtler number $G\ddot{o}_\theta \sim 7.1$–8.1 and when the vortices were amplified to an amplification factor in the range $e^{5.5} \leq A \leq e^7$.

The minimum nondimensional wavelength of 215 achieved in this experiment was limited by turbulent flow through insufficient side wall boundary-layer removal. Consequently, it cannot be concluded that $\Lambda \approx 200$ is the minimum *possible* wavelength. For example, if a larger gap were used, the turbulent boundary layer could be removed at the lower suction limits (i.e., velocity ratios $U_G/U_\infty < 0.76$). That is, the lower limit may be geometry dependent. The only theoretical limitation is that the wavelengths must be greater than $\Lambda \sim 50$. It may be possible to achieve $\Lambda < 200$ for freestream velocities $U_\infty \neq 500$ cm/s, but this has not been explored extensively.

The maximum spacing remained relatively constant at 8 ± 1 low-speed streaks ($\lambda \sim 2.5$ cm) for velocity ratios greater than $U_G/U_\infty \sim 1$ at $U_\infty = 500$ cm/s. Therefore, it appears that the effects of suction on controlling the spacing of Görtler vortices become saturated above some suction level.

The exact process of wavelength selection is not well-understood at this time. The variation of suction may alter the pressure gradient at the leading edge, the initial radius of curvature of the streamlines near the leading edge, or some other unknown variable that affects the selection of the wavelength.

Acknowledgment

This work was sponsored by the Air Force Office of Scientific Research under Contract F49620-85-C-0080 monitored by J. McMichael. This support is gratefully acknowledged.

References

[1]Görtler, H., "Über Eine Dreidimensionale Instabilität Laminarer Grenzschichten an Konkaven Wänden," *Math, Phys. Klasse*, Vol. 2, 1940, pp. 1–26, also NACA TM-1375, 1954.

[2]Herbert, T., "On the Stability of the Boundary Layer Along a Concave Wall," *Archiwum Mechaniki Stosowanej*, Vol. 28, No. 5–6, 1976, pp. 1039–1055.

[3]Floryan, J. M., and Saric, W. S., "Stability of Görtler Vortices in Boundary Layers," *AIAA Journal*, Vol. 20, No. 3, 1982, pp. 316–324.

[4]Floryan, J. M., and Saric, W. S., "Wavelength Selection and Growth of Görtler Vortices," *AIAA Journal*, Vol. 22, No. 11, 1984, pp. 1529–1538.

[5]Bippes, H., "Experimentelle Untersuchung des Laminar-Turbulenten Unschlags an Einer Parallel Angestromten Konkaven Wand," *Sitzungsberichte der Heidelberger Akademie der Wissenschaften Mathematisch-Naturwissenschaftliche Klasse*, No. 3, 1972, pp. 103–180; also NASA TM-75243, 1978.

[6]Winoto, S. H., and Crane, R. I., "Vortex Structure in Laminar Boundary Layers on a Concave Wall," *International Journal of Heat and Fluid Flow*, Vol. 2, No. 4, 1980, pp. 221–231.

[7]Ito, A., "Breakdown Structure of Longitudinal Vortices Along a Concave Wall," *Transactions of the Japan Society of Aeronautical and Space Science*, Vol. 33, March 1985, pp. 166–173.

[8]Aihara, Y., and Koyama, H., "Secondary Instability of Görtler Vortices: Formation of Periodic Three-Dimensional Coherent Structure," *Transactions of the Japan Society of Aeronautical and Space Science*, Vol. 24, Aug. 1981, pp. 78–94.

[9]Tani, I., "Production of Longitudinal Vortices in the Boundary Layer Along a Concave Wall," *Journal of Geophysical Research*, Vol. 67, No. 8, 1962, pp. 3075–3080.

[10]Tani, I., and Sakagami, J., "Boundary-Layer Instability at Subsonic Speeds," *Proceedings of Third Congress of International Council of Aerospace Sciences, Stockholm 1962*, Spartan, Washington, DC, 1964, pp. 391–403.

[11]Swearingen, J. D., and Blackwelder, R. F., "Spacing of Streamwise Vortices on Concave Walls," *AIAA Journal*, Vol. 24, No. 10, 1986, pp. 1706–1709.

[12]Tani, I., and Aihara, Y., "Görtler Vortices and Boundary-Layer Transition," *Zeitschrift Fur Angewandte Mathematik Und Physik*, Vol. 20, No. 5, 1969, pp. 609–618.

[13]Aihara, Y., Tomita, Y., and Ito, A., "Generation, Development,

and Distortion of Longitudinal Vortices in Boundary Layers Along Concave and Flat Plates," *IUTAM Symposium Novosibirsk/1984 Laminar-Turbulent Transition*, Springer-Verlag, New York, 1985, pp. 447–454.

[14]Swearingen, J. D., and Blackwelder, R. F., "The Growth and Breakdown of Streamwise Vortices in the Presence of a Wall," *Journal of Fluid Mechanics*, Vol. 182, Sept. 1987, pp. 255–290.

[15]Liepmann, H. W., "Investigation on Boundary-Layer Transition on Concave Walls," NACA Wartime Rept. W-87, Feb. 1945.

[16]Smith, A. M. O., "On the Growth of Taylor-Görtler Vortices Along Highly Concave Walls," *Quarterly Journal of Applied Mathematics*, Vol. 13, No. 3, 1955, pp. 233–262.

[17]Winoto, S. H., and Low, H. T., "Transition of Boundary-Layer Flows in the Presence of Görtler Vortices," *Experiments in Fluids*, Vol. 8, No. ½, 1989, pp. 41–47.

[18]Bippes, H., "Experimental Results on the Görtler-Instability Problem and Comparison with Theoretical Approaches," *Colloquium on Görtler Vortex Flows, EuroMech 261*, Nantes, France, 1990.

[19]Park, D., "The Primary and Secondary Instabilities of Görtler Flow," Ph.D. Thesis, Univ. of Southern California, CA, 1990.